

International Conference on Space Optics—ICSO 2018

Chania, Greece

9–12 October 2018

Edited by Zoran Sodnik, Nikos Karafolas, and Bruno Cugny



Digital correction of residual straylight in FLEX images

S. Abdon

D. Armand

F. Laurent

M. Barillot

et al.



Digital correction of residual straylight in FLEX images

S. Abdon - D. Armand - F. Laurent - M. Barillot (Thales Alenia Space France)
A. D'Ottavi - P. Coppo - E. De Luca - R. Gabrieli (Leonardo)
M. Bouvet - M. François - M. Taccola (ESA/ESTEC)

ABSTRACT

The FLEX mission is defined to perform quantitative measurements of the solar induced vegetation fluorescence to monitor photosynthetic activity. The FLORIS payload is based on a spaceborne 3-channel grating spectrometer operating in the VNIR range.

The retrieval of the faint fluorescence signal from the acquired vegetation spectra is particularly sensitive to straylight.

As results, the straylight requirements on the FLORIS instrument are especially stringent.

For FLORIS a two-step straylight reduction process has been put in place by the Leonardo-Thales Alenia Space team to achieve this requirement. Careful instrument design and manufacturing are followed by digital processing of the raw instrument data.

In this paper we present the feasibility demonstration of the straylight digital correction process, based on simulation of the dedicated data processing and quantitative assessment of the residuals.

Keywords: hyperspectral, spectro-radiometer, fluorescence, space, straylight, analysis, correction, processing

1 THE FLEX MISSION

1.1 Overview

The FLuorescence EXplorer (FLEX) mission has been selected for the European Space Agency (ESA) Earth Explorer EE8 program¹. The FLEX mission is defined to perform quantitative measurements of the solar induced chlorophyll fluorescence (Figure 1) to monitor the photosynthetic efficiency of the terrestrial vegetation layer². As complement to traditional reflectance measurements, fluorescence estimates provide an early and more direct approach for diagnosing carbon assimilation and the health status of vegetation. Applications include farming, forest management, and assessment of the terrestrial carbon budget.

The FLEX measurements are performed from space by the FLuORescence Imaging Spectrometer (FLORIS)³. The FLEX payload will be mounted on a medium/small size platform and fly in a Sun synchronous orbit at a height of about 815 km, in tandem with one of the Copernicus Sentinel-3 satellites. Synergy with visible reflectance and surface temperature data are provided by Sentinel-3's instruments, respectively the Ocean and Land Colour Imager (OLCI⁴) and the Sea and Land Surface Temperature Radiometer (SLSTR⁵).

The contract for the Phase B2/C/D/E1 of the FLORIS development has been awarded by ESA to the Leonardo Company (Italy) as prime contractor and OHB AG System (Germany) as core team sub-contractor. Phase B2 included extensive pre-development activities⁶ and was completed in September 2018 with the instrument Preliminary Design Review (PDR). A feasibility study of the digital correction of straylight was awarded by Leonardo to Thales Alenia Space for phase B2; most of the work reported here was performed in the framework of this feasibility study.

International Conference on Space Optics—ICSO 2018

Chania, Greece

9–12 October 2018

Edited by Zoran Sodnik, Nikos Karafolas, and Bruno Cugny



Digital correction of residual straylight in FLEX images

S. Abdon

D. Armand

F. Laurent

M. Barillot

et al.



ics0 proceedings



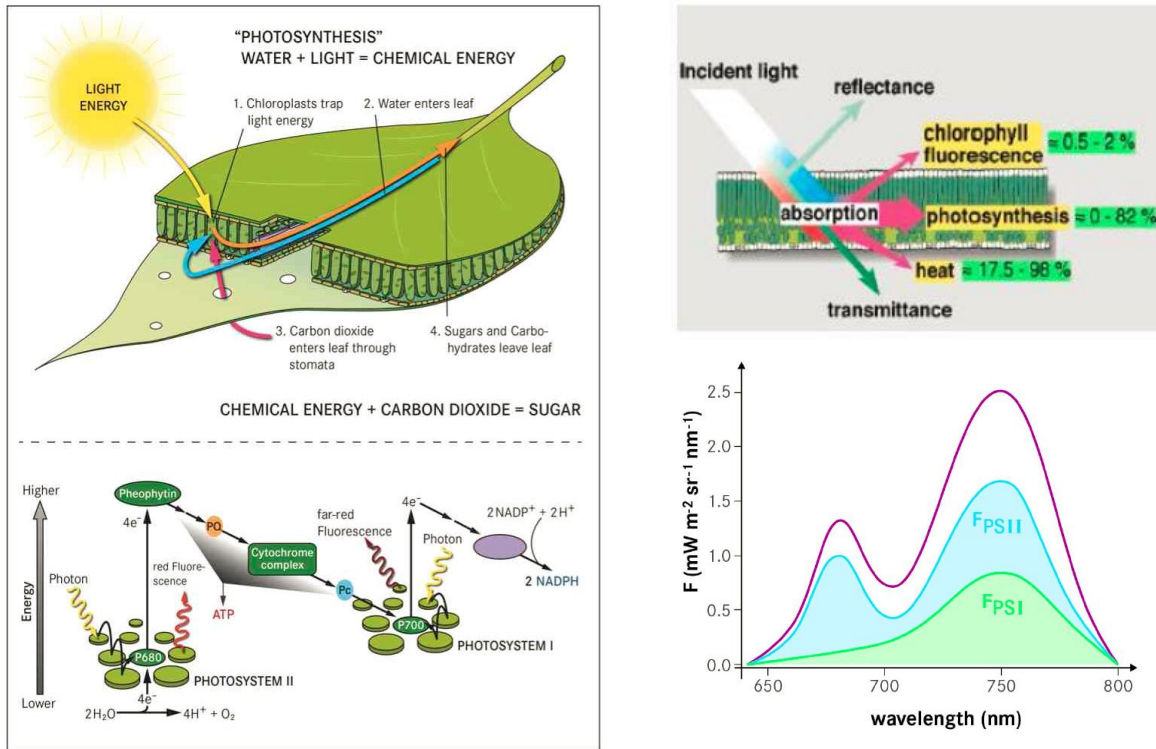


Figure 1: The chlorophyll fluorescence process

1.2 Straylight requirements at L1b: spatial and spectral

As shown in Figure 1, the fluorescence spectral radiance averages about $2\text{mW}/\text{m}^2/\text{sr}/\text{nm}$ only, which typically represents two orders of magnitude less than the Earth reflectance signal. Algorithms are therefore necessary to extract the fluorescence signal from the total observed signal. They make use of the large variation of the solar illumination in the spectral range of the O₂A (within 740-780nm) and O₂B (within 677-697nm) atmospheric absorption windows. The FLEX mission aims at measuring fluorescence with 10% of accuracy. As the accuracy of the algorithm is particularly sensitive to the presence of straylight, the maximum acceptable levels lie two further orders of magnitude below the fluorescence signal, at $0.04\text{mW}/\text{m}^2/\text{sr}/\text{nm}$. All in all the rejection efficiency of the straylight generated by the Earth reflectance signal must reach four orders of magnitude.

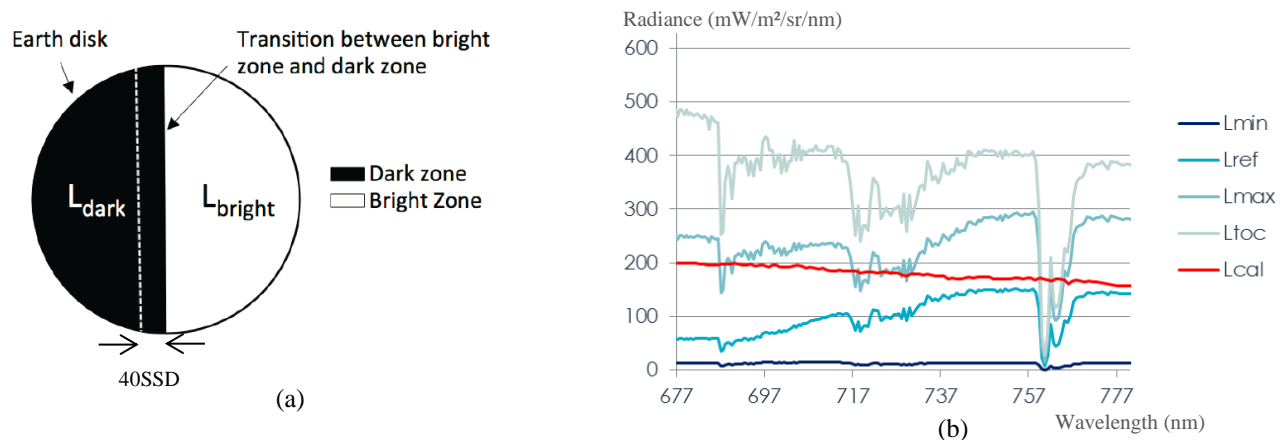


Figure 2: Specified Non Uniform scene (a) and non-uniform spectra (b) for stray-light performance evaluation.

The reference straylight scenes for quantitative assessment of the straylight performance have been spatially and spectrally defined by ESA as reported in Figure 2. In the spatial dimension, the straylight must meet the requirement at 40 Spatial Sampling Distance (SSD) from the radiance transition. In the spectral dimension, the transitions are determined from the Earth reflectance radiance tables.

2 FLORIS HARDWARE

FLORIS is a pushbroom spectrometer based on diffraction gratings and matrix CCD detectors, where one direction is used for swath and the other for spectral separation. As shown in Figure 3, a common 234.5 mm, f/3.1 telescope illuminates two spatially separated Offner spectrometers over a field-of-view (FoV) of $\pm 5^\circ$ corresponding to a 150km swath on ground. The High Resolution (HR) Spectrometer has a spectral resolution of 0.3nm and sampling interval of 0.1nm; it covers both O₂A and O₂B atmospheric absorption windows with the help of two separate CCD arrays. The Low Resolution (LR) Spectrometer has a spectral resolution of 1.8nm and sampling interval of 0.6nm ; it covers the 500-758nm spectral range.

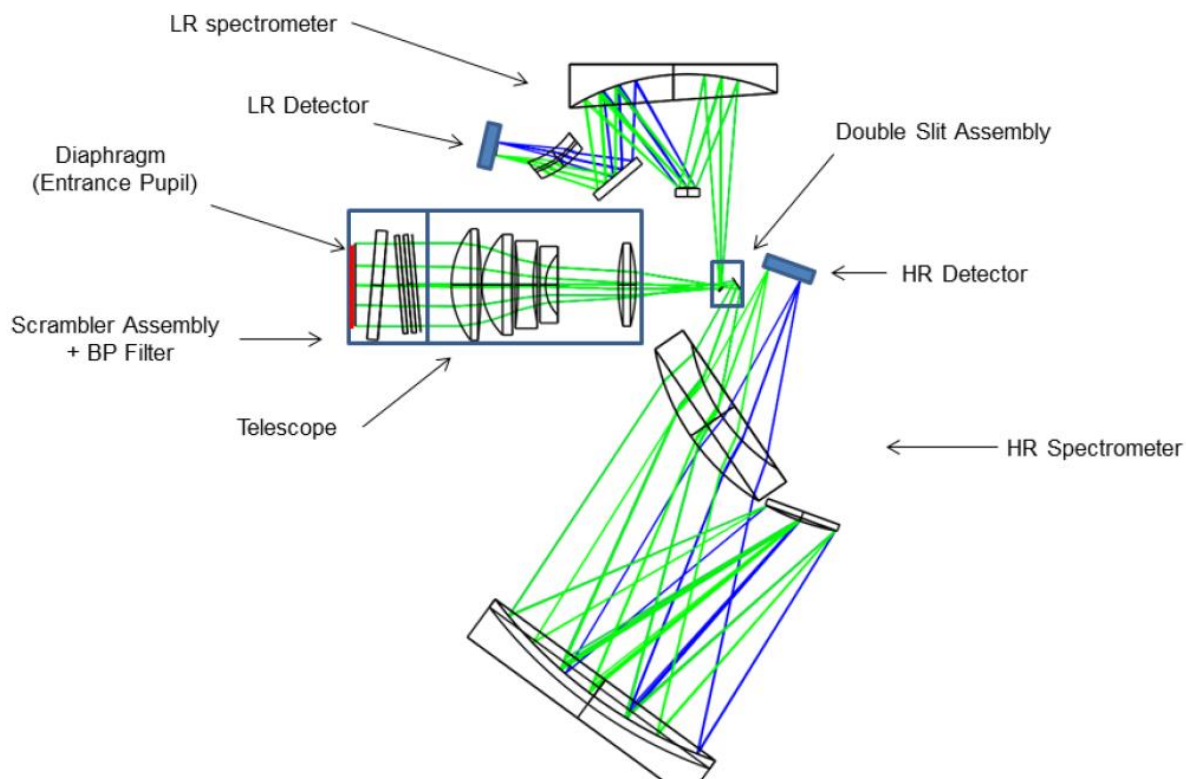


Figure 3: FLORIS Optical layout at start of phase B2

In order to reduce straylight to a very low value before post-corrections of straylight by on-ground image processing are implemented, ESA has set a stringent requirement of 0.2mW/m²/sr/nm, five times the above mentioned mission requirement, on the instrument hardware capability of rejecting straylight. As results several dedicated solutions have been implemented.

The FLORIS design involves a reduced number of optical surfaces. As ghost image reduction was made a strong driver of the telescope design, the telescope lenses have been reduced from 8 to 5 at a moderate optical quality cost. Further optimisation will be performed until Telescope PDR. The particularly critical HR Spectrometer includes only one single meniscus lens in dual path, reducing ghosts to a nearly acceptable level. An optional Linear Variable Filter (LVF) may be introduced in front of the HR detectors if needed without design modification.

In addition to the natural blocking effect of the spectrometer slit, careful baffling is implemented in both direct and solar calibration configurations of the instrument in order to shadow out-of-scene straylight sources and block spurious light paths. A light trap is also accommodated in the path of the zero diffraction order of the HR grating.

Excellent roughness and transmission efficiency of the optical surfaces comes from the use of state-of-the-art polishing and anti-reflective coatings technologies. In the same spirit, high performance blackening solutions are foreseen where reflections or scattering by mechanical surface may occur.

Scattering by particulate contamination (PAC) is kept to a similar level as roughness thanks to a drastic Cleanliness and Contamination Control Plan, which takes into account all integration and test activities until the satellite launch. The inclusion of the telescope lenses into a virtually tight cylinder helps achieve a nearly non-contaminated PAC level on most of the optical surfaces. Overall the budgeted PAC levels range from 35ppm to 250ppm depending on the surface exposure to the outside of the instrument and the cleaning capability. We demonstrated that the probability of particle re-distribution at launch to modify the scattering properties of the surfaces and jeopardize the on-ground calibration/verification of the straylight is very low. Should it nevertheless happen, in-flight calibration/verification on the lunar disk is planned as baseline during the in-orbit commissioning.

3 HARDWARE PERFORMANCE

The straylight performance plots presented in Figure 4 (a) and (b) represent the starting point of the straylight correction assessment which we are presenting here. They are excellent as the straylight induced signal is about three orders of magnitude below the actual signal of the reference scene (a typical vegetation spectrum). In recent instruments, the straylight levels typically exceed one percent of the direct image. However, both spectrometer and telescope straylight remain significantly above the mission straylight requirement.

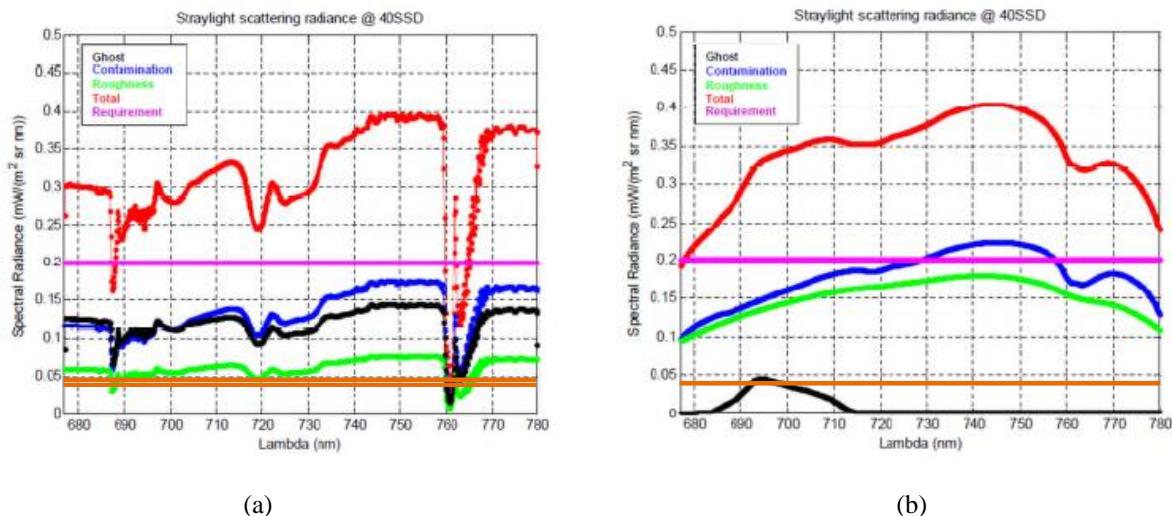


Figure 4: Computed straylight performance (a) telescope (b) HR spectrometer
Pink line: hardware requirement –Brown line: mission requirement

These plots also show that telescope and spectrometer straylight levels are approximately of the same amplitude. Furthermore, on the telescope side, the respective weights of ghosts and scattering remain balanced.

On the spectrometer side, ghosts are dominated by scattering, but remain quantitatively slightly above the mission requirement.

Overall, quantitatively speaking, the telescope and spectrometer straylight combine for more than 0.6mW/m².sr.nm, i.e. 3 times the hardware requirement of 0.2mW/m².sr.nm, and 15 times the mission requirement of 0.04mW/m².sr.nm.

As results, on-ground digital correction of the residual straylight is necessary to meet the straylight requirement. It must be able to divide the hardware induced straylight by a factor of about 15, a quite challenging value. Furthermore, as on-ground calibration, among others, also contribute to the residual straylight, we allocated a maximum residual uncertainty of 3% of the hardware straylight to the inaccuracies of the digital processing operations.

Recently, improvements of the optical design have further reduced the straylight by a factor of up to 2, depending on the wavelength. Nevertheless the statement that a highly efficient digital correction needs to be implemented remains valid.

4 CORRECTION APPROACH

As image formation is basically a convolution process between the observed object, or scene, and the PSF of the instrument, which includes a straylight component named Straylight Point-Spread Function (SPSF), straylight digital correction is based on a deconvolution process involving the image and straylight maps as kernel.

Deconvolution is a computationally demanding mathematical process. In practice, thanks to the relatively weak straylight power compared to the image, the deconvolution can be replaced by a lighter approximation, as explained in the present subsection.

The developments make use of the following definitions:

- Scene radiance: I_S
- Measured radiance: I_M
- Straylight radiance: I_{stray}
- Point Spread Function: PSF
- Straylight included in the PSF (or $SPSF$): A_{stray}

The signal measured by the instrument is the sum of the signal coming from the scene and the straylight signal :

$$I_M = I_S + I_{stray} \quad (1)$$

Straylight correction is performed to retrieve the signal coming from the scene. It merely consists in a subtraction:

$$I_S = I_M - I_{stray} \quad (2)$$

The straylight signal results from a convolution process. Using $*$ as the convolution operator we may write :

$$I_{stray} = A_{stray} * I_S \quad (3)$$

As results from (2) and (3):

$$I_S = I_M - (A_{stray} * I_S) \quad (4)$$

As I_S is unknown (we actually try to retrieve I_S), we will use I_M instead. The resulting formula writes:

$$I_S \approx I_M - (A_{stray} * I_M) \quad (5)$$

The associated approximation of eq. (4) can be estimated as follows:

$$\begin{aligned} I_M - (A_{stray} * I_M) &= I_M - (A_{stray} * (I_S + I_{stray})) \\ &= I_M - (A_{stray} * I_S) - (A_{stray} * A_{stray} * I_S) \end{aligned} \quad (6)$$

Eq. (6) shows that the difference between the exact expression of eq. (4) and the approximated eq. (5) is limited to the term $(A_{stray} * I_{stray})$ which represents “the straylight from the straylight”. In a properly design instrument, $I_{stray} \ll I_S$ therefore $(A_{stray} * I_{stray})$ is of the second order compared to the straylight itself (in the FLORIS case, below 0.6%), which justifies the approximation.

In general, the mathematical operation is not strictly a deconvolution as the kernel A_{stray} varies over the FoV and spectrum. In practice, the variations of the straylight kernel over the complete ACross-Track (ACT), ALong-Track (ALT) and spectral ranges of the instrument are built from a small set of supposedly perfect Straylight Point Spread Functions (SPSF). In the present phase B2 approach a preliminary set has been computed by means of an optical model of the instrument. In the future, the operational set is planned to result from carefully calibrated measurements of the flight instrument ; therefore for practical reasons the number of input SPSF in the set can only be very limited.

Then one or several reference SPSF are provided at as different locations as possible from the reconstruction set in the (ACT, ALT, spectrum) data cube. The reconstruction accuracy is assessed from the integrated difference of the reference case and the reconstructed ones.

5 CORRECTION OF SCATTERED STRAYLIGHT

As scattered straylight is expected to be quite slowly variable over the FoV, the reconstruction is supposed to be simpler than in the case of ghosts. For this reason, we tested the reconstruction efficiency based on as limited a set of SPSF as spectrometer and telescope scattering kernels (SPST_tel and SPST_spec) at 686nm and 758nm. Telescope and spectrometer PSF are supposed to be uniform over the FoV. Out of field sources are attenuated according to a baffle vignetting function.

5.1 SPSF Reconstruction error

For an in-field source, the reconstruction efficiency at 720nm (approximately midway from the known set) is excellent as illustrated in Figure 5. Similar computations using different, but still uniform, PSF inputs yield similar results.

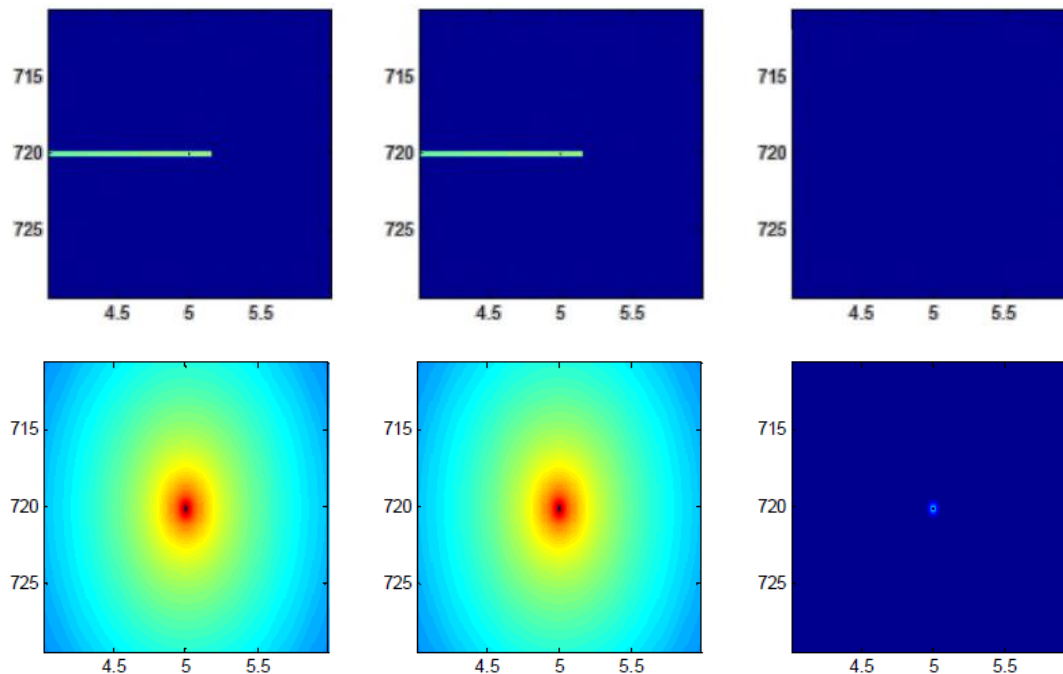


Figure 5: Comparison between reference SPSF (left), reconstructed SPSF (centre) and difference. Top: telescope SPSF masked by the slit and imaged in the detector plane; bottom: spectrometer illuminated from a perfect telescope. Integrated reconstruction accuracy = 0.1% (telescope) and 0.3% (spectrometer). Vertical axis: wavelength - Horizontal axis: ACT FoV [°] – Color scale: normalised to 1

As seen from the instrument focal plane, most of the telescope straylight is blocked by the spectrometer slit. This explains why the first line of Figure 5 looks linear; the important result here is that the reconstructed PSF of the telescope nearly perfectly matches the reference.

5.2 Out-of-field and out-of-band straylight contribution

The contribution of out-of-field sources to the straylight can hardly be corrected as a priori no information is available from the instrument data regarding the intensity of these sources. The performance essentially relies on the baffling efficiency of the instrument. Assuming a uniform scene, we computed the respective proportions of straylight coming from inside and outside the FoV. The results (Figure 6) show that the out-of-field straylight exceed 2% of the in-field straylight in the outer areas of the FoV only. As the FoV is oversized with respect to the mission needs, the impact of out-of-field straylight into the mission swath is acceptable.

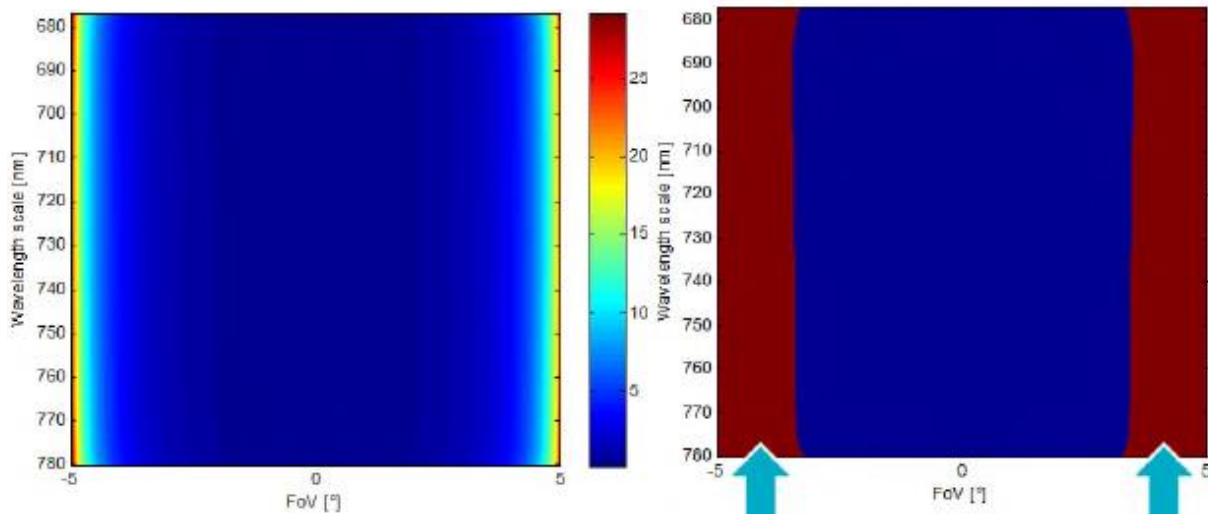


Figure 6: Left: Out-of-FoV straylight compared to total straylight in %. Right: areas where the Out-of-FoV straylight exceeds 2% of the total straylight.

These results confirm the adequacy of the instrument design. Significant potential for improvement exist as knowledge of the Out-of-FoV sources may bring the possibility to correct the Out-of-FoV straylight too. The use of OLCI image data would be particularly appropriate as the very large FoV OLCI flies on-board Sentinel-3 in formation with FLEX and shares spatial resolution as well as spectrum with FLORIS. The short time lag between both instruments virtually cancels the variations of the clouds between both instrument images. Nevertheless, this option would significantly increase the complexity of the FLEX ground segment.

Straylight may also come from Out-of-Spectral range light sources. The availability of data from the large spectral range FLORIS LR spectrometer brings the possibility to correct straylight from wavelengths outside the HR spectrometer range, except above 758nm, which brings the situation shown in Figure 7. Figure 7 assumes that the slope of the spectral cut-off filter which blocks light beyond 780nm is 15nm.

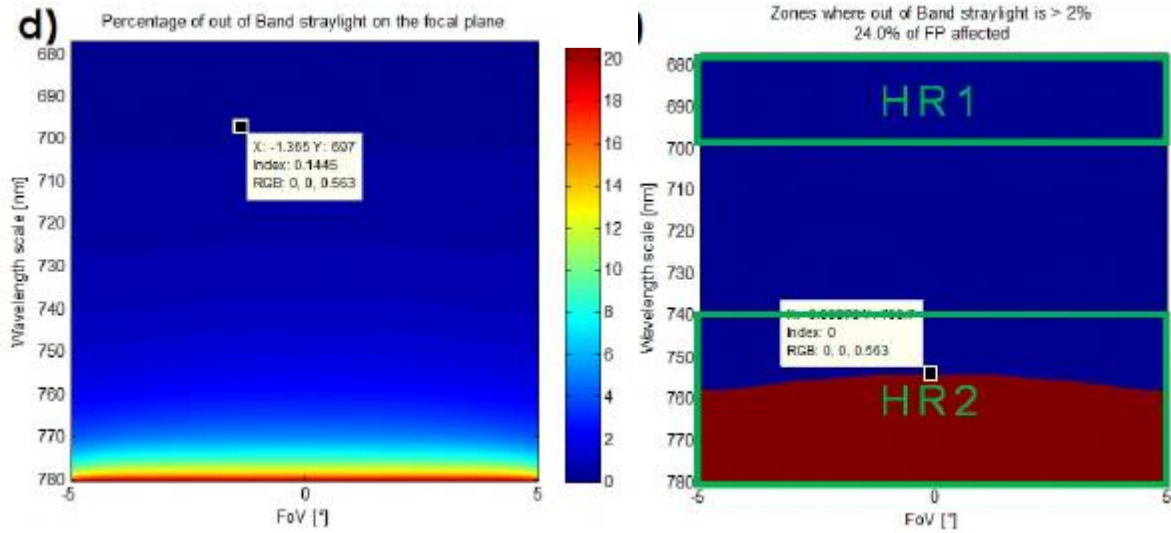


Figure 7: Left: Out-of-spectral range straylight compared to total straylight in %. Right: areas where Out-of- spectral range straylight exceeds 2% of total straylight.

Here again, the performance may be improved by the use of OLCI image data as the OLCI spectrum goes up to 1040nm. Simpler solutions are also possible, such as improving the slope of the spectral cut-off filter. Extrapolating the spectral contents of the scene in the limited range where the cut-off filter is not fully efficient is also a quite attractive option for recovering enough knowledge of the straylight source. This extrapolation is possible thanks to the relatively smooth behaviour of the spectrum in 770-800nm range according to used reference spectra (see Figure 8).

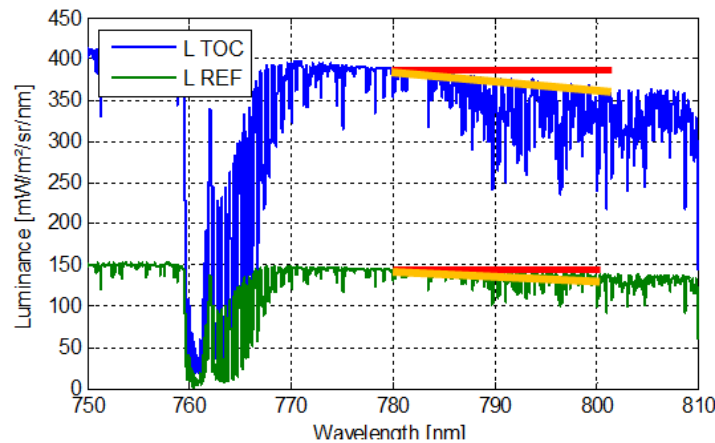


Figure 8: Out of band spectrum extrapolation. Red line: constant extrapolation of last value; Orange line linear extrapolation based on 770-780nm data.

6 CORRECTION OF TELESCOPE GHOSTS

Image ghosts show sharper and less predictable variations over the FoV. How many input SPSF will be necessary to provide enough information for a consistent build-up of the correction kernel is a key question. As far as telescope ghosts are concerned, our analysis was based on the set of input SPSF shown in Figure 9. Accurate knowledge of 12 SPST functions are therefore sufficient to achieve the correction performance shown here.

Wavelength	686nm	691.5nm	697nm
FoV (deg)	TEL	TEL	TEL
0	1	3	1
0,49	2	3	2
0,97	1	3	1
1,47	2	3	2
1,95	1	3	1
2,44	2	-	2
2,93	1	-	1
3,42	2	-	2
3,91	1	-	1
4,88	1	-	1

Figure 9: Input SPSF for building up the correction of telescope ghosts. In green: set of SPSF used for kernel reconstruction. In blue: reference set points used for testing the reconstruction efficiency. The numbers merely indicate the delivery batch.

Ghost correction efficiency is illustrated in Figure 10 for the reference point (1.47°, 691.5nm). Our model predicts the strongest ghost accurately enough so that considering the correction of the second strongest ghost is not even necessary to achieve the efficiency objective.

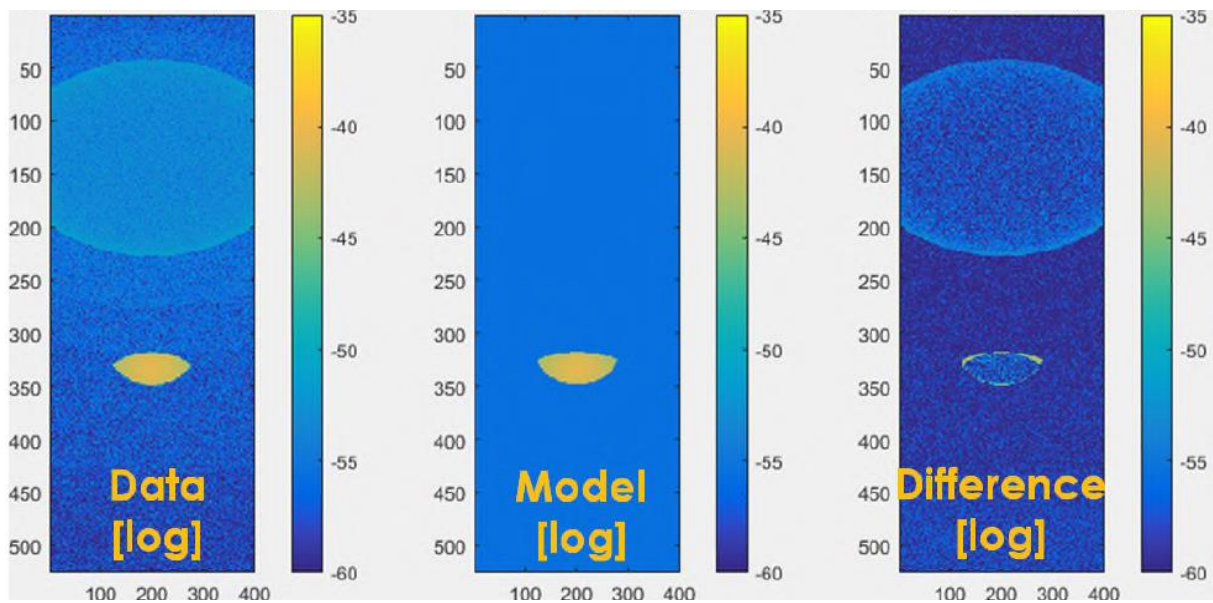


Figure 10: Comparison between telescope ghosts reference SPSF (left), reconstructed SPSF (centre) and difference. Log scales.

After correction, the residual power essentially consists of noise from the reference SPSF. The uncorrected secondary ghosts, although quite visible in log scale, carries a secondary contribution. Overall, the correction efficiency accuracy is everywhere better than 80%, as shown in Figure 11.

Wavelength FoV (deg)	ε %		
	686nm	691.5nm	697nm
0	14,5	14,6	14,5
0,49	15,5	15,4	19,1
0,97	15,4	15,7	15,6
1,47	17,1	17,1	17,4
1,95	17,5	17,7	17,6
2,44	17,8	-	18,1
2,93	17,4	-	17,3
3,42	15,5	-	15,5
3,91	13,6	-	13,6
4,88	15,7	-	15,0

Figure 11: Residue of telescope ghost correction

Although the correction does not divide the straylight by 15, the demonstrated factor of approximately 6 or more is sufficient, taking into account that the telescope ghosts represent only a fraction of the total straylight. Furthermore, less noisy inputs would mechanically bring better results. Finally, there remains room for improvement as the second strongest ghosts could be included in the model.

Fundamentally, these good results are actually made possible thanks to the relatively smooth behaviour of the ghost over the FoV and spectrum.

7 CORRECTION OF THE SPECTROMETER GHOSTS

By contrast with the telescope ghosts, the spectrometer ghosts exhibit a line shape, as illustrated in Figure 12 for the stronger one.

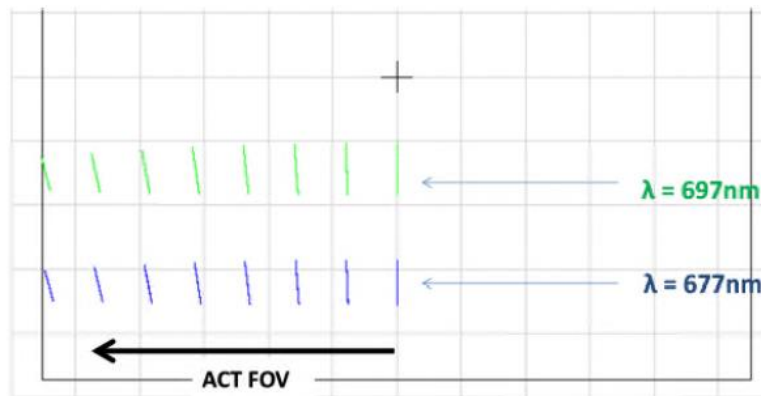


Figure 12: Spectrometer ghosts for 2 different wavelengths and 8 positions in the FoV

This unusual behaviour is consistent with the measurements on the FLORIS breadboard⁶. It is explained by the astigmatic nature of the propagation of ghosts generated within an Offner arrangement where the various optical surfaces are concentric. Thanks to the reduced number of surfaces, the individual ghosts of the spectrometer have been analysed one by one using FRED (Figure 13).

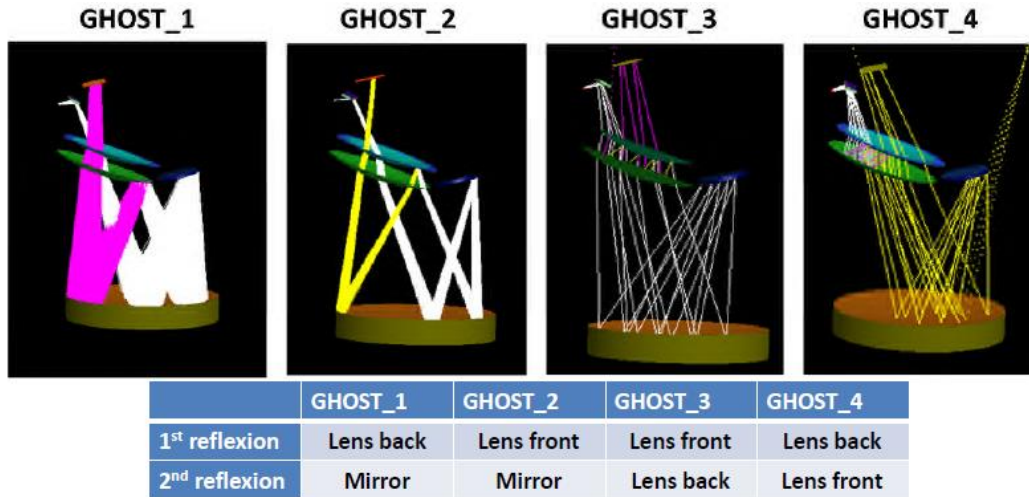


Figure 13: Formation of ghost images within the FLORIS HR spectrometer

Despite this sharp geometry, we have been able to develop a correction tool from a limited number of input SPSF, as indicated in Figure 14.

Wavelength	Spectrometer				
	686 nm	688,75	691,5	694,25	697
FoV (deg)					
0	1	-	1	-	1
0,49	-	-	4	-	-
0,97	1	-	1	-	1
1,47	-	-	4	-	-
1,95	1	-	1	-	1
2,44	4	-	4	-	4
2,93	1	-	1	-	1
3,42	4	4	4	4	4
3,91	1	4	1	4	1
4,4	5	4	4	4	4
4,88	1	-	1	-	1

Figure 14: Input SPSF for building up the correction of spectrometer ghosts. Same colour code and number meaning as in Figure 9.

The correction efficiency is illustrated in Figure 15 for the reference point (4.4°, 688.75nm).

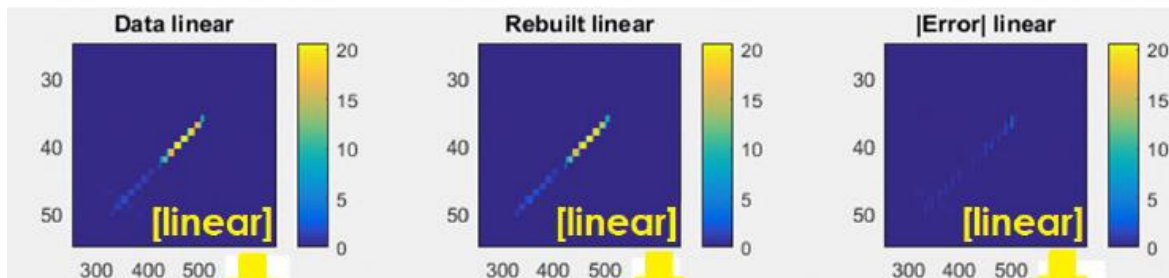


Figure 15: Comparison between spectrometer ghosts reference SPSF (left), reconstructed SPSF (centre) and difference. Linear means linear amplitude scales. X-axes: ACT direction [in detector pixel number]; Y-axes: spectral direction [in detector pixel number]

After correction, the ghosts are attenuated by approximately 88%. Taking advantage of the extremely thin nature of the ghost images, further improvement were achieved by averaging the opposite sides of the ghosts lines, at the cost of some acceptable blurring from the image quality requirements point of view. As results, the correction efficiency exceeds 95% in nearly all cases (Figure 16).

Wavelength	sum_line(sum_columns(ERROR)) (%)				
FoV (deg)	686 nm	688,75	691,5	694,25	697
0	5,48	-	4,26	-	4,60
0,49	-	-	4,24	-	-
0,97	4,43	-	4,06	-	4,23
1,47	-	-	3,60	-	-
1,95	3,04	-	3,07	-	3,04
2,44	2,64	-	2,61	-	2,61
2,93	3,24	-	3,43	-	3,66
3,42	2,77	2,80	2,88	3,03	3,21
3,91	3,84	3,43	4,03	3,62	4,49
4,4	3,96	4,05	4,14	4,31	4,80
4,88	4,84	-	5,09	-	6,12

Figure 16: Residue of HR spectrometer ghost correction

It is reminded here that in case the development of this unusual tool would lead to disappointing results, the implementation of a Linear Variable Filter would present a definitive alternative. A 10nm wide LVF would indeed cut all the spectrometer ghosts off, at the cost of additional ghosts, with a more conventional shape, introduced by the LVF itself.

8 CONCLUSION

The correction efficiency of the digital tools we have developed is sufficient to meet the mission needs of reducing the currently modelled hardware straylight down to a less than 3% residue. The significant ghost images generated inside the telescope and spectrometer have been taken into account. The build-up of the correction tools is based on a moderate quantity of inputs, compatible with a test and measurement campaign on the ground. The presence of uncorrected noise in the inputs provides further margin to the quantitative estimations of the residues.

These very encouraging results should not hide the fact that deriving accurate instrument characterisation data from on-ground measurement to feed the straylight correction will represent a challenge as well as ensuring that state-of-the-art computational solutions and cleanliness methods are implemented.

References

- [1] Drusch, M.; Moreno, J.; Del Bello, U.; Franco, R.; Goulas, Y.; Huth, A.; Kraft, S.; Middleton, E.M.; Miglietta, F.; Mohammed, G.; et al. The Fluorescence Explorer Mission Concept—ESA’s Earth Explorer 8. *IEEE Trans. Geosci. Remote Sens.* 2017, 55, 1273-1284, doi:10.1109/TGRS.2016.2621820.
- [2] Meroni, M.; Rossini, M.; Guanter, L.; Alonso, L.; Rascher, U.; Colombo, R.; Moreno, J. Remote sensing of solar-induced chlorophyll fluorescence: Review of methods and applications. *Remote Sens. Environ.* 2009, 113, 2037–2051.
- [3] Coppo P., A. Taiti, L. Pettinato, M. Francois, M. Taccola and M. Drusch, Fluorescence Imaging Spectrometer (FLORIS) for ESA FLEX Mission, Special Issue "Remote Sensing of Vegetation Fluorescence and Photosynthetic Efficiency" (ISSN 2072-4292), *Remote Sens.* 2017, 9, 649; MDPI editor, doi:10.3390/rs9070649.
- [4] Nieke, J.; Borde, F.; Mavrocordatos, C.; Berruti, B.; Delclaud, Y.; Riti, J.B.; Garnier, T. The Ocean and Land Colour Imager (OLCI) for the Sentinel 3 GMES Mission: Status and first test results. *Proc. SPIE* 2012, 8528, 85280C.
- [5] Coppo, P.; Ricciarelli, B.; Brandani, F.; Delderfield, J.; Ferlet, M.; Mutlow, C.; Munro, G.; Nightingale, T.; Smith, D.; Bianchi, S.; et al. SLSTR: A high dual scan temperature radiometer for sea and land surface monitoring from space. *J. Mod. Opt.* 2010, 57, 1815–1830, doi:10.1080/09500340.2010.503010.
- [6] Pettinato, L.; Fossati, E.; Coppo, P. M.; Taiti, A.; Labate, D.; Capanni, A.; Taccola, M., Bézy, J. L.; François, M.; Meynart, R.; Erdmann, L.; Triebel, P.; Instrument pre-development activities for FLEX. *Proc. SPIE* 2017, 10423, 1042305-1